

Novel metal chelates with thiourea and nicotinic acid: Synthesis, structural characterization, and biological properties

Sanaa M. Emam^a, Saeyda A. AbouEl-Enein^a, Sanaa A. Othman^b and Eman M. El-Mahdey^{b*}

^aChemistry Department, Faculty of Science, Menoufia University, Shebin El-Kom, Egypt

^bSoil, Water and Environmental Research Institute Agriculture Research Center, Egypt

CHRONICLE

Article history:

Received July 18, 2022

Received in revised form

August 25, 2022

Accepted December 14, 2022

Available online

December 14, 2022

Keywords:

Nicotinic acid

Thiourea

Metal Chelates

IR

Biological Studies

ABSTRACT

The interaction of nicotinic acid and thiourea with the chloride salts of Ca(II), Mg(II), Co(II), Ni(II), Cu(II), and Fe(III) ions led to the synthesis of a unique series of metal chelates. All formed metal complexes were clarified using a variety of analytical and spectral techniques, besides magnetic moment and thermal tests. The electronic and magnetic measurements indicated that the paramagnetic chelates (3) and (4), as well as the diamagnetic complexes (1) and (2), were responsible for the tetrahedral geometrical structure. The outcomes also led to the production of square-planar, and high-spin octahedral structures for chelates (5) and (6). Thermodynamic studies using activation energy values revealed that complex (1) is more thermally stable than complex (2) and complex (3) is more stable than complex (4). Fe(III) complex exhibits higher antibacterial and antifungal activities than other metal complexes. Chelate (6) exhibits the highest rate of germination in wheat.

© 2023 by the authors; licensee Growing Science, Canada.

1. Introduction

Nicotinic acid is an organic compound, otherwise called vitamin B₃ or Niacin. It is a colorless solid water-soluble. Nicotinic acid and its derivatives are strong organic multidentate chelating ligands, most of them coordinate with the metal ions through the lone pair of electrons in nitrogen and oxygen atoms.¹ Further, it is used to reduce cholesterol levels and lower the risk of heart disease.² Spraying of nicotinic acid increases plant growth and biomass weight. Therefore, foliar sprays appear to mitigate the negative effects of increased salinity.³ This type of ligands and their metal chelates have many important biological activities like anticancer, antibacterial, antifungal, antiviral, and anti-inflammatory⁴⁻¹¹ as well as they are found to be pharmacologically and physiologically active. Niacin plays an important role in the cell breath, arrival of energy, working of the nervous system, and typical discharge of bile and stomach,¹² it may help to prevent skin cells from sun damage well as applied as a lotion and it may help prevent some types of skin cancer.^{13,14} Some metal chelates of nicotinic acid and its derivatives have supramolecular association via hydrogen or covalent bonds.^{5,15} In industry, Niacin is used as an anticorrosion agent for mild steel¹⁶, in the chemical polishing of steel under high-temperature conditions¹⁷, and as an organic catalyst.¹⁸

Thiourea, also known as a thiocarbamide contains three functional groups, amino, imino, and thiol. On the other hand, the importance of complexes including thiourea is due to their biological activities involving antimicrobial, antiviral, antitumor, anti-nociceptive, and insecticidal activities along with their uses in several medicines, and agriculture applications. In addition, thiourea is utilized to improve plant growth under normal and stressful conditions as well as

* Corresponding author.

E-mail address emahdey.eman@yahoo.com (S. M. Emamhas)

coordinating agents due to the existence of oxygen, nitrogen, and sulfur donor atoms.¹⁹⁻²⁵ Thiourea is used in several applications in industry as in the processing of gold²⁶ and as a corrosion inhibitor.²⁷

A lack of Ca and Mg in wheat results in stunted roots, leaves that do not turn yellow, necrotic spotting in the middle of the youngest leaf, and leaf collapse and unrolling. Ca and Mg are essential to plant macronutrients that are required for the growth, functionality, and health of root tips and meristems. Also, Fe is a micronutrient for plant growth, its deficiency led to new leaves being affected first and becoming chlorotic.^{28,29} In addition, metal ions are also essential to our life as organic molecules. Zn(II), Ca(II), and Mg(II) ions, for example, can be employed to prevent the development of cancer and are found in large quantities in metallothionein proteins as well as in live organisms. The cellular system's RNA and DNA are connected to the divalent ions Ca, Mg, Fe, Cu, and Mn, which support the biological functions of the nucleus. Additionally, magnesium is used to provide energy to enzymes in both plants and animals.³⁰ Numerous plants are affected by fungus-related illnesses^{31,32}, so that in these reports all encourage us to create metal chelates, including nicotinic acid, and thiourea which react with various metal chlorides. Various spectroscopic and analytical methods were used to clarify the structure of these compounds. They were also used as a growth promoter for wheat and to explore their biological effects against *Fusarium oxysporum f.sp. betae* fungi and *Erwinia carotovora* sp. *carotovora* bacteria.

2. Experimental

2.1. Materials and Physical Measurements

All chemicals used were chemically pure grade and were utilized without further purification. $\text{CoCl}_2 \cdot 6\text{H}_2\text{O}$, $\text{CuCl}_2 \cdot 2\text{H}_2\text{O}$, $\text{NiCl}_2 \cdot 6\text{H}_2\text{O}$, $\text{MgCl}_2 \cdot 6\text{H}_2\text{O}$, CaCl_2 , and $\text{FeCl}_3 \cdot 6\text{H}_2\text{O}$ salts have been employed. Elemental analyses (C, H, N) were carried out on the Perkin Elmer-2400 elemental analyzer at Micro Analytical Center, Faculty of Science- Cairo university. Metal ions of the prepared complexes have been determined by complexometric titration using EDTA and the percentage of chloride ions within the complexes was indirectly estimated by Mohr's method.³³ The solution of the investigated metal ions were prepared by boiling (0.08g) of complexes with concentrated HNO_3 acid mixed with concentrated HCl (v/v:1:3), then followed by the addition of distilled water affording a clear solution. Thermogravimetric analysis (TG/DTG) were performed using a Shimadzu DAT/TG-50 thermal analyzer with a heating rate of $10^\circ\text{C}/\text{min}$ under an N_2 atmosphere with a flowing rate of 20 mL/min from room temperature up to 900°C using platinum crucibles. Johnson Matthey's magnetic susceptibility balance was used to measure magnetic susceptibilities employing the Gouy method. The diamagnetic corrections were calculated using Pascal's constants.³⁴ The effective magnetic moments were calculated as Bohr Magneton from the equation $\{\mu_{\text{eff}} = 2.84(\chi M^{\text{corr}})^{1/2}\}$. The ^1H NMR spectrum was measured in DMSO-d₆ on a DELTA-2 NMR spectrometer at 500 MHz. Infrared spectra of the metal chelates were demonstrated on a Thermo-Fisher Nicolette FT-IR spectrophotometer within range ($400\text{--}4000\text{cm}^{-1}$). The Perkin-Elmer Lambda 4B spectrophotometer was employed to measure the electronic absorption spectra in Nujol mulls. Mass spectrometry instruments for metal complexes (Ca, Cu, Fe, and Co) were performed on a Shimadzu Qp-2010 Plus spectrometer. Molar conductivities of all metal complexes were measured at room temperature in DMSO solution (10^{-3}M) using a type ORION 4 STAR (PH – conductivity Benchtop) conductometer. The melting points were measured with the Stuart melting point apparatus.

2.2. Preparation of Metal Complexes of Nicotinic acid and Thiourea using the Template method

A hot ethanolic solution (15mL) of one mole of nicotinic acid (3g) was added to an equimolar of ethanolic solution (15mL) of thiourea (1.85g). The reaction mixture was stirred under reflux for 2 hours at (70°C). After that, an ethanolic solution (10 mL) of equimolar of metal chloride salts including bivalent metals, $\text{MCl}_2 \cdot n\text{H}_2\text{O}$ (M: Ca, n=0; Mg, n=6; Co, n=6; Ni, n=6 and Cu, n=2) and $\text{FeCl}_3 \cdot 6\text{H}_2\text{O}$ were added with continuous stirring to the reaction mixture and refluxed at (70°C) for 8 hours. The formed precipitate was filtered off, and washed with ethanol, and dried. Afterward, all prepared compounds were crystallized by boiling in absolute ethanol, filtered, and dried under a vacuum over anhydrous CaCl_2 .

2.3. Biological Activity

The antimicrobial activity of some metal complexes was estimated against *Fusarium oxysporum f.sp. betae* fungi and *Erwinia carotovora* sp. *carotovora* bacteria at Plant Pathology Research Institute, Agriculture Research Center, Egypt. Complexes (1), (2), and (6) were utilized with different concentrations, then, they were mixed with different ratios. The bactericidal activities of these compounds were investigated using the agar plate technique³⁵ on (*Erwinia carotovora* sp. *carotovora*) plant pathogenic bacteria. In addition, these compounds were studied against fungi (*Fusarium*) using potato dextrose agar (PDA).³⁶

The agriculture applications experiment was conducted during the 2021 winter season, using wheat (Egypt 2) in sandy soil. Irrigation was performed for 15 days employing different prepared complexes (Ca, Mg, Fe, and mixture from these chelates) in different concentrations (50, 150, 250 ppm). These results were compared to distilled water (control). After the planting intervals, germination rate, and green, dry weight were recorded. Metal concentrations of Ca, Mg, and Fe were measured by using a standard EDTA solution and the mixture ions were identified using the Inductive Coupled Plasma (ICP) mass spectrometry instrument, Perkin Elmer Model: Optima 7000 DV. Nitrogen concentration was measured using

the Kjeldahl procedure.³⁷ Agriculture measurements were evaluated at Soil, Water and Environmental Research Institute, Agriculture Research Center, Egypt.

3. Results and discussion

3.1. Characterization of Nicotinic acid and Thiourea Metal Complexes

Analytical Data

The physical and analytical results of nicotinic acid, thiourea, and their metal complexes are tabulated in (**Table S1**). The structure of the formed compounds was elucidated via microanalyses, spectral studies, thermal (TG/DTG), magnetic and molar conductance measurements. The metal chelates obtained from the reaction of nicotinic acid and thiourea with different metal salts are separated with different stoichiometry. All metal complexes are stable, non-hygroscopic, and partially soluble in aprotic organic solvents, but they are freely soluble in DMSO. The molar conductance measurements recorded in (10^{-3} M) DMSO solution established that all chelates are typified (1:1) electrolytes, within the range; 49.1-79.2 $\Omega^{-1} \text{ cm}^2 \text{ mol}^{-1}$.^{38,39}

3.2. IR Spectra of Nicotinic Acid, Thiourea, and their Metal Complexes

Tables S2 and S3 summarize the infrared frequencies and their assignments for thiourea, nicotinic acid, and their metal complexes, respectively. The IR spectra of all metal chelates are shown in **Fig. (S1)**. By comparing the main fundamental infrared spectral bands of the prepared metal chelates to the spectra of the parent ligands (thiourea and nicotinic acid), it was found that:

The IR spectral data displayed (C=NH) group which is formed from tautomerism that occurred in thiourea moiety and observed in the chemical structures of all complexes except complex (**5**), but the other type of azomethine group is created from the condensation reaction between the carbonyl group of nicotinic acid and NH_2 group which is found in thiourea.⁴⁰ However, the spectra of chelates demonstrate new bands appeared at ($1617\text{--}1635 \text{ cm}^{-1}$) characterized to $\nu(\text{C}=\text{N})$; these types of bands are overlapped with $\nu(\text{C}=\text{O})$ in Co(II), Ni(II), and Cu(II) complexes.

The results of IR showed that the different vibrations of NH_2 group (ν and δ) disappeared in all metal chelates except in Cu(II) complex, confirming that the condensation process which occurs between NH_2 of thiourea and carbonyl group of nicotinic acid takes place. On the other hand, the $\delta(\text{NH}_2)$ that was observed at 1587 cm^{-1} appeared in Cu(II) complex with broadness and shift to lower frequency supporting its involvement in inter and intramolecular hydrogen bonding.⁴¹⁻⁴³

The lower shift of $\nu(\text{C}=\text{O})$ and the higher shift of $\gamma(\text{C}=\text{O})$ are observed at ($1691\text{--}1714$) and ($500\text{--}555$) cm^{-1} , respectively, typified the participation of carbonyl oxygen atom in chelation.³⁹ This is confirmed by the appearance of a new vibrational band at the same frequency assigned to $\nu(\text{M}-\text{O})$ (**Table S3**).

All metal chelates spectra exhibit different modes of vibrations for (OH) located at ($1310\text{--}1332$), ($1247\text{--}1300$), and ($1036\text{--}1048$) cm^{-1} , which are ascribed to $\delta(\text{OH})$ and $\gamma(\text{OH})$, respectively.⁴⁴ These bands illustrate that one of the nicotinyl moieties is attached to the metal ion in its protonated form (OH group). However, the $\gamma(\text{OH})$ of nicotinyl moiety (956 cm^{-1}) disappeared in all complexes, except in Ca(II) and Mg(II) complexes. Also, the OH group of other nicotinyl species chelated with all metal ions in its deprotonated form except in Ca(II) and Mg(II) complexes.

Also, the spectra of complexes illustrated weak and strong bands that appeared within range ($1562\text{--}1596$) and ($1403\text{--}1422$) cm^{-1} attributed to $\nu_a(\text{COO}^-)$ and $\nu_s(\text{COO}^-)$, respectively.¹⁹ This ascertains the presence of nicotinate moiety bonded with the metal ion. In some chelates, the asymmetric stretching vibrations of (COO^-) have been obscured with $\{\nu(\text{C}=\text{C})+\nu(\text{C}=\text{N})\}$ of the pyridine ring.

The spectra of all metal complexes revealed $\nu(\text{SH})$ and $\nu(\text{C}-\text{S})$ spectral bands observed at ($2576\text{--}2632$) and 744 cm^{-1} , associated with negative and positive shifts respectively, relative to the corresponding bands in thiourea. This is supporting the participation of (SH) sulfur atom in bonding with all metal ions.⁴⁵⁻⁴⁸

3.3. Electronic Spectra of Metal Complexes

The electronic spectra of metal complexes were measured in Nujol mull at room temperature. The electronic spectra and effective magnetic moment values (μ_{eff} B.M.) are represented in **Table (S4)** and **Fig. (S2)**. The electronic spectra of all metal complexes display medium bands at $226\text{--}242$, $272\text{--}328$; $328\text{--}471$, and $388\text{--}471 \text{ nm}$. The first three bands are assigned to $\pi-\pi^*$ and $n-\pi^*$ electronic transitions, but the four band is due to LMCT transition.⁴⁹

The electronic spectra of diamagnetic Mg(II) and Ca(II) complexes show three bands at 239 , $328\text{--}342$, and $433\text{--}456 \text{ nm}$. The first and the second bands correspond to electronic transition which is denoted by bonding and antibonding orbital ($\pi-\pi^*$) in the pyridine ring, and (C=O) group along with (C=N) group. Also, the later peak is assigned to $n-\pi^*$ transition that occurred due to the existence of C=O and C=N groups.⁵⁰

The electronic spectrum of cobalt(II) complex clarifies bands at 545, 623 assignable to ${}^4A_2(F) \rightarrow {}^4T_1(P)$ and ${}^4A_2(F) \rightarrow {}^4T_1(F)$ transitions, respectively. This points to tetrahedral geometry around cobalt(II) ions. The tetrahedral structure of Co(II) complex (**3**) (**Fig. S2**) was confirmed by the magnetic moment value ($\mu_{\text{eff}} = 4.66$ B.M.) which agrees well with the tetrahedral environment around Co(II) ion.^{49,51}

The electronic spectrum of Ni(II) complex exhibits three bands at 640, 688, and 743 nm ascribed to ${}^3T_1(F) \rightarrow {}^3T_1(P)$, ${}^3T_1(F) \rightarrow {}^3A_2(F)$, and ${}^3T_1(F) \rightarrow {}^3T_2(F)$ transitions, respectively. The magnetic moment value of Ni(II) complex (**4**) was measured giving 4.24 B.M. which was consistent with two unpaired electrons confirming the tetrahedral geometry around Ni(II) ion.^{52,53}

The electronic spectrum of copper(II) complex (**5**) depicts broad bands at 510 and 596 nm assigned to ${}^2B_{1g} \rightarrow {}^2E_g$ and ${}^2B_{1g} \rightarrow {}^2A_g$, respectively. The magnetic moment value is found to be (1.42 B.M.) indicating the square-planar structure.⁵⁴⁻⁵⁶

The high spin octahedral Fe(III) possesses a d^5 configuration that denotes only the magnetic moment value corresponding to the spin-only (5.9 B.M.). This is due to the absence of orbital angular contribution from the ground state (6F). Also, the lower value of magnetic moment (4.68 B.M.) for complex (**6**) is due to metal-metal interaction and the spin cross-over phenomena.⁵⁷ The electronic spectrum of Fe(III) complex (**6**) exhibits peaks at 472, 503, and 564 nm assignable to ${}^6A_{1g} \rightarrow {}^4A_{1g}(G)$, ${}^4E_g(G)$, ${}^6A_{1g}(S) \rightarrow {}^4T_{2g}(G)$ and ${}^6A_{1g}(S) \rightarrow {}^4T_{1g}(G)$, respectively, indicating high spin octahedral iron(III) complex.^{53,58,59} The lower magnetic moment values for copper(II) and iron(III) complexes established the existence of metal-metal interaction.⁵⁹

3.4. ${}^1\text{H}$ NMR Spectra of Ca(II) Complex

The ${}^1\text{H}$ NMR spectrum of Ca(II) complex (**2**) is displayed in **Fig. (S3)** as supplementary information. It was performed in DMSO giving a weak signal at 13.38 ppm assigned to the OH proton of the nicotinic acid moiety.⁶⁰ The signal due to OH proton (-COOH) in the Schiff base is absent, referring to its involvement in coordination with the metal ion after deprotonation. On the other hand, a broad weak signal appears at 3.47 ppm assignable to coordinated water.⁶¹ The signals due to pyridine ring protons were observed as two doublet, one multiple and one singlet at (8.76-8.77, 8.24-8.26); (7.54-7.51) and 7.16 ppm, respectively.^{60,62} Based on the integration value (2.00) (**Fig. S3**), it was observed that the two protons characterized to C=NH and SH appeared as one strong signal at 9.05 ppm.^{63,64}

3.5. Mass Spectra for Metal Complexes

Fast atom bombardment (FAB) mass spectroscopy analysis of complexes CaCl_2 , CoCl_2 , CuCl_2 , and FeCl_3 were performed and the assignment of their fragments is listed in **Table (S5)**. The molecular ion peaks of these complexes were observed at $m/e = 431.47, 448.33, 553.98, \text{ and } 644.61$, respectively.

The spectrum of calcium(II) chloride complex (**Fig. S4**) shows species at $m/e = 431.20, 361.19, 265.20, 189.10, 148.10, 104.15, 68.15$ and 56.10 amu, indicating to $[\text{C}_{14.5}\text{H}_{17.5}\text{N}_4\text{O}_{4.75}\text{SCaCl}]^+$, $[\text{C}_{13}\text{H}_{13}\text{N}_4\text{O}_4\text{SCa}]^+$, $[\text{C}_8\text{H}_8\text{N}_3\text{O}_3\text{SCa}]^+$, $[\text{C}_3\text{H}_5\text{N}_2\text{O}_3\text{SCa}]^+$, $[\text{C}_2\text{H}_4\text{O}_3\text{SCa}]^+$, $[\text{CH}_4\text{O}_3\text{Ca}]^+$, $[\text{CaO}+\text{C}]^+$ and $[\text{CaO}]^+$, respectively.

The spectrum of cobalt(II) chloride chelate (**Fig. S5**) showed fragments at $m/e = 448.10, 424.10, 397.10, 362.10, 253.10, 177.10, 123.10, 105.10$ and 82.10 amu, corresponding to $[\text{C}_{15}\text{H}_{17.5}\text{N}_4\text{O}_{4.25}\text{SCoCl}]^+$, $[\text{C}_{14}\text{H}_{14.5}\text{N}_4\text{O}_{3.75}\text{SCoCl}]^+$, $[\text{C}_{13}\text{H}_{11}\text{N}_4\text{O}_3\text{SCoCl}]^+$, $[\text{C}_{13}\text{H}_{11}\text{N}_4\text{O}_3\text{SCo}]^+$, $[\text{C}_8\text{H}_8\text{N}_3\text{O}_3\text{Co}]^+$, $[\text{C}_3\text{H}_6\text{N}_2\text{O}_3\text{Co}]^+$, $[\text{CH}_4\text{O}_3\text{Co}]^+$, $[\text{CH}_2\text{O}_2\text{Co}]^+$ and $[0.5(\text{Co}_2\text{O}_3)]^+$, respectively.

Besides, The spectrum of copper(II) chloride complex (**Fig. S6**) donates different fragmentations at $m/e = 553.70, 539.45, 482.75, 387.40, 310.80, 226.10, 196.50, 123.10, 78.05$ and 63.95 amu, referring to $[\text{C}_{13}\text{H}_{19}\text{N}_4\text{O}_8\text{SCu}_2\text{Cl}]^+$, $[\text{C}_{13}\text{H}_{17.5}\text{N}_4\text{O}_{7.25}\text{SCu}_2\text{Cl}]^+$, $[\text{C}_{13}\text{H}_{15}\text{N}_4\text{O}_6\text{SCu}_2]^+$, $[\text{C}_8\text{H}_{10}\text{N}_3\text{O}_5\text{SCu}_2]^+$, $[\text{C}_3\text{H}_7\text{N}_2\text{O}_5\text{SCu}_2]^+$, $[\text{CH}_7\text{O}_5\text{Cu}_2]^+$, $[\text{H}_5\text{O}_4\text{Cu}_2]^+$, $[\text{H}_4\text{O}_{3.5}\text{Cu}]^+$, $[\text{CuO}]^+$ and $[\text{Cu}]^+$, respectively.

Furthermore, the FAB spectrum of iron(III) chloride chelate (**Fig. S7**) showed fragments at $m/e = 644.10, 621.10, 409.10, 332.10, 260.10, 176.10, 123.10$ and 112.20 amu, denoting to $[\text{C}_{14.5}\text{H}_{20.5}\text{N}_4\text{O}_{6.75}\text{SFe}_2\text{Cl}_4]^+$, $[\text{C}_{13.5}\text{H}_{17.5}\text{N}_4\text{O}_{6.25}\text{SFe}_2\text{Cl}_4]^+$, $[\text{C}_8\text{H}_9\text{N}_3\text{O}_3\text{SFe}_2\text{Cl}_2]^+$, $[\text{C}_3\text{H}_6\text{N}_2\text{O}_3\text{SFe}_2\text{Cl}_2]^+$, $[\text{C}_2\text{H}_6\text{O}_3\text{Fe}_2\text{Cl}_2]^+$, $[\text{CH}_4\text{O}_3\text{Fe}_2]^+$, $[\text{Fe}_2\text{C}]^+$ and $[2\text{Fe}]^+$, respectively.

3.6. Thermal Analysis for Metal Complexes

Thermal analysis may be a very useful technique to limit the thermal stability of compounds, confirm molecular formulas, and decide the various forms of crystallized solvent molecules. This measurement is employed to suggest a general mechanism for the thermal decomposition of those complexes. **Fig. 1** and **Table 1** clarify the TG and DTG thermal degradation of all metal chelates. The TG curve of complexes reveals two and three thermal decomposition steps for complexes (**4**) and (**1, 2, 5**), respectively. The decomposition of all metal complexes began at low temperatures (20-30°C), which may be related to the solvent of crystallization inter/intramolecular hydrogen bonding with the coordination sphere.

Metal oxide for complexes (1, 5, and 6), and metal oxide polluted with carbon are the ultimate remnants determined by the thermal decomposition for complexes (2, 3, and 4).

The structural properties of metal complexes and the assortment of metal ions influence the thermal behavior of the desolvation /decomposition step in metal chelates. This study can be clarified by calculating the activation energy (E_a), the order of reaction (n), and the activation enthalpy (ΔH), using the analysis of the DTG curves. The order of reaction (n) can be determined using the DTG curve.⁶⁵ The activation energy values (E_a) for the desolvation/decomposition stage can be calculated using the initial rate method,^{66,67} where $\ln I$ was plotted versus $(1000/T)$ for the low-temperature peak affording a straight line with a slope equal to $(-E_a/R)$, where I represents $(d\alpha/dt)$ in the DTG curve and ΔT in the DTA curve.^{41,65,67} Also, the parameters (ΔH , ΔS , and ΔG) were estimated from these equations: $\Delta H = E^* - R\Delta T$; $\Delta S^* = RT \ln(Ah/KT)$; $\Delta G = \Delta H - T\Delta S^*$, where K , h , R , A , and T are Boltzmann's, Planck's and gas constants, frequency factor and absolute temperature, respectively. The thermodynamic and kinetic parameters of the metal complexes are given in **Table 2**. The TG measurements were performed at a heating rate of $10^\circ\text{C}/\text{min}$ under nitrogen within the temperature range of 20 - 900°C .

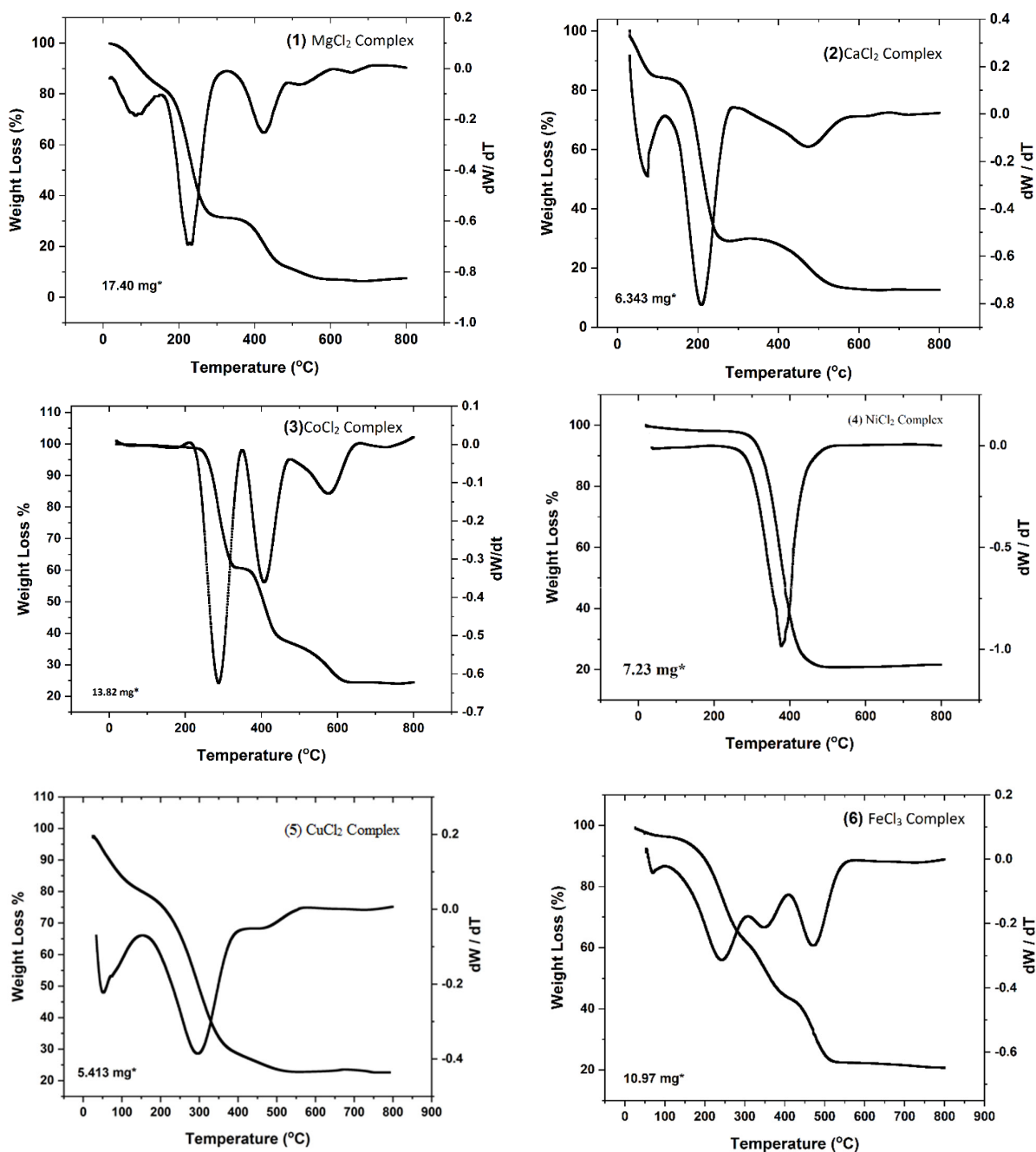
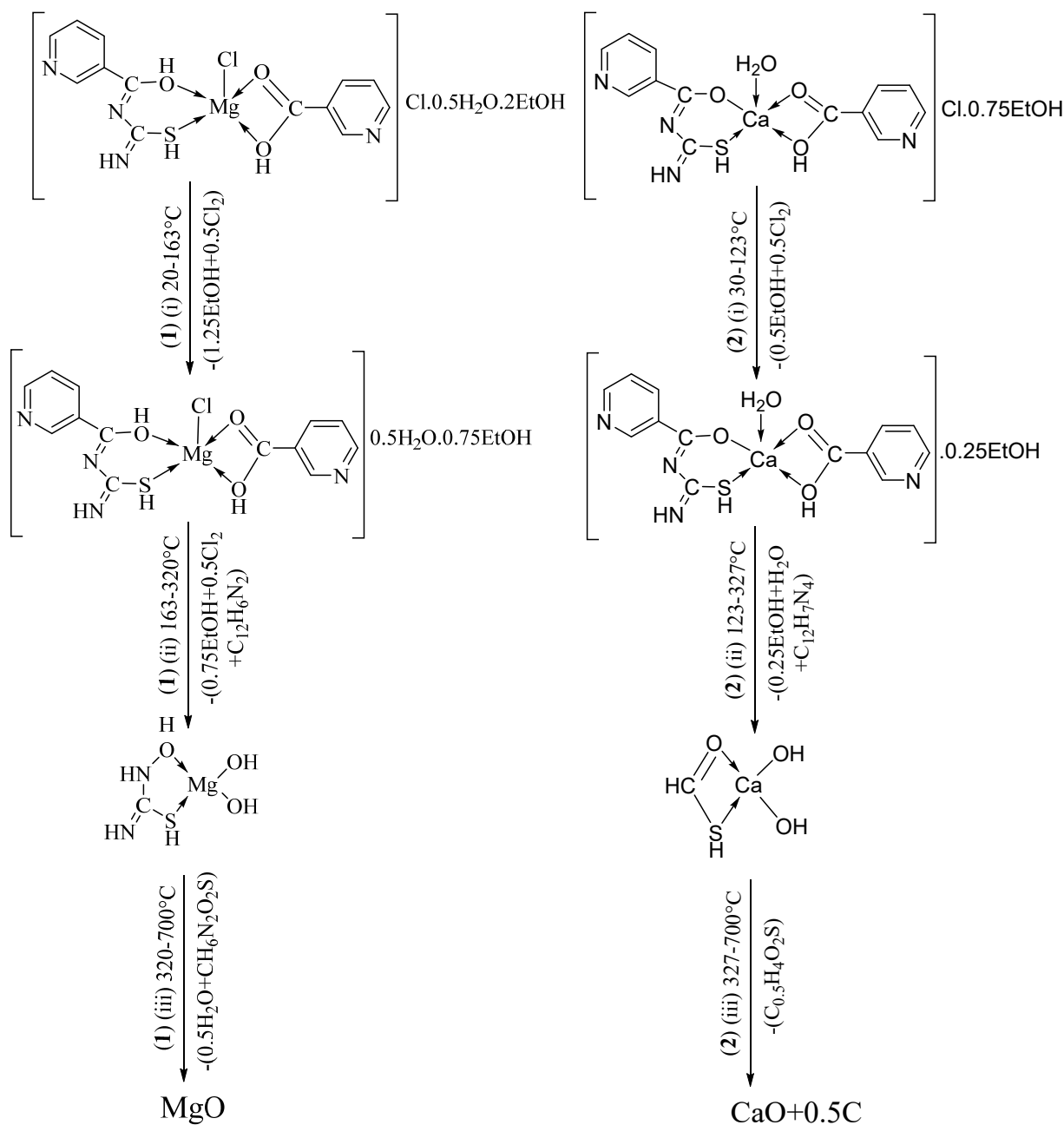
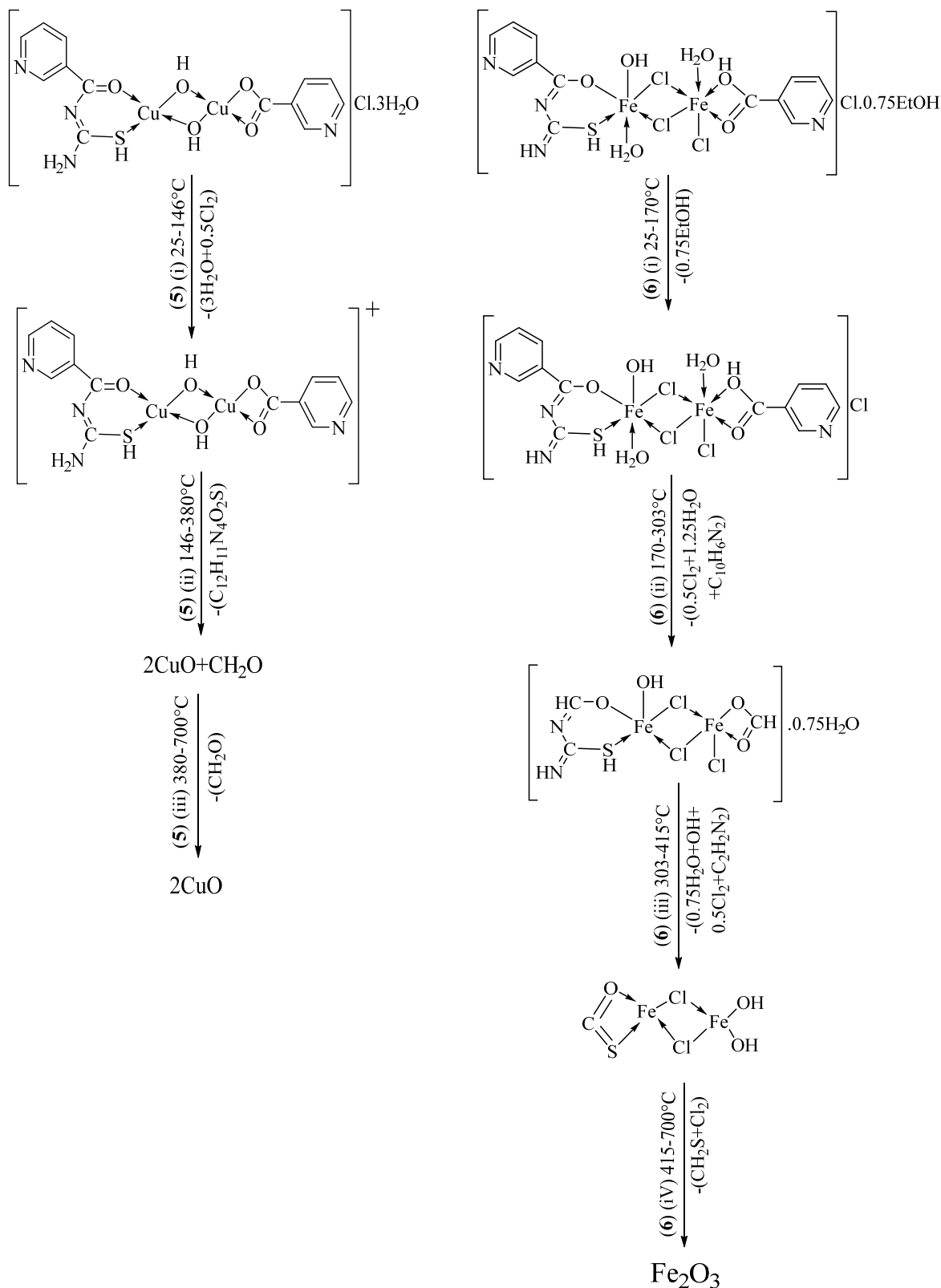


Fig. 1. TG/DTG Curves of metal complexes derived from nicotinic acid and thiourea

The TG-DTG curves of complexes (1) and (2) are demonstrated in **Fig. 1** revealing their thermal decomposition in a similar pathway including three steps (**Scheme 1**). The first desolvation step is observed at temperature ranges 20-163 and 30-123°C, associated with weak DTG peaks at (T_{max} =88 and 54°C), corresponding to the removal of 1.25 mol of EtOH and 0.5 mol of EtOH as well as the elimination of ionic chloride ion for complexes (1) and (2), respectively (**Scheme 1**). The low-temperature extension for this decomposition is demonstrative of the elimination of adsorbed lattice solvent in chelated compounds. In this event, the ease of releasing these dissolved particles is credited to weak interaction within the crystal voids. The estimated activation energies for this stage are found 22.29 and 30.0 KJmol⁻¹ for complexes (1) and (2), respectively (**Table 2**). After that, the remaining crystallized solvent molecules (0.75 mol and 0.25 mol of EtOH); the coordinated anions (Cl and H₂O), and two mol of pyridyl moieties associated with 2C and C₂H₂N₂ are eliminated in the second decomposition step within temperature range (123-327°C). This stage is accompanied by two strong DTG peaks at (T_{max} = 228 and 209°C) with kinetic first order along with activation energy values of 87.01 and 72.32 KJmol⁻¹ for complexes (1) and (2), respectively. Finally, this stage is followed by complete delegation with the removal of the remaining lattice water (0.5 H₂O) in complex (1) with mass losses of 24.48% and 17.05% for complexes (1) and (2), respectively. This step is associated with two broad weak DTG peaks at (T_{max} = 424 and 473°C), ended with the formation of magnesium oxide and calcium oxide contaminated with carbon for complexes (1) and (2), respectively (**Table 1**).³⁰



Scheme 1. Suggested thermal decomposition of complexes (1) and (2)



Scheme 3. Suggested thermal decomposition of complexes **(5)** and **(6)**

The TG curves of Cu(II) and Fe(III) complexes **(5, 6)** demonstrated three and four decomposition steps within ranges (25-700°C) and (26-700°C), respectively (**Schemes 3** and **4**). The first one is noted at (25-146°C) and (26-170°C) associated

with weak DTG peaks at (T_{max} =63 and 48°C) assignable to the elimination of (three mol of crystallized H₂O and half mol of Cl₂ gas) for complex (5) with mass loss of (16.17 %) and 0.75 mol of EtOH for complex (6). The counted activation energy values and kinetic order reaction are (30.79 KJ.mol⁻¹, 1.74) and (18.78 KJmol⁻¹, 1.9) for complexes (5) and (6), respectively, (Table 2). This step is followed by the second one at temperature ranges (146-380°C) and (170-303°C) and described by two strong DTG peaks at (T_{max} =300 and 242°C). This event is ascribed to the loss of two pyridyl moieties (2C₅H₃N) for both chelates and (C₂H₅N₂O₂S) for complex (5) along with the removal of (1.25 mol) of coordinated H₂O molecules, and coordinated anions (Cl ion) for complex (6) (Table 1). Also, this step is characterized by activation energy values 61.64 and 54.19 KJmol⁻¹ for complexes (5) and (6), respectively. In addition, for chelate (5), the second step is followed by complete delegation with mass loss of (5.57%) and strong DTG peak at 401°C affording two mol of CuO as a final product.^{31,44} This step is described by activation energy value 58.48 KJmol⁻¹ and kinetic order reaction 1.41. On the other hand, complex (6) completes its degradation in the third and fourth steps within temperature ranges 303-415 and 415-700°C pointing to the elimination of the remaining coordinated water, coordinated OH, chloride ions, and (C₃H₅N₂S) forming Fe₂O₃ as final residue.⁵² These steps are accompanied by medium and strong DTG peaks observed at (T_{max} =348 and 471°C) and characterized by estimated activation energy values 125.19 and 96.82 KJmol⁻¹, as well as kinetic order reaction 1.45.

3.7. Kinetic and Thermal Stability Studies

Based on the TG studies (Table 1) and calculation of activation energy values (Table 2) for most of the thermal decomposition steps of metal chelates, it was concluded that:

The thermal degradation of complexes (1) and (4) has higher thermal stability and decomposition occurs at higher temperatures in comparison with that of complexes (2) and (3), respectively. Table 2 demonstrates a regular increase in activation energy values of complex (1) in comparison with those for complex (2), this is indicative of the higher thermal stability of complex (1). This may be due to the smaller ionic size and higher electronegativity of Mg(II) than those of Ca(II). This behavior can be explained by the higher covalency for the Mg-L bond than that in the Ca-L bond. In addition, the higher thermal activity of chelate (1) than complex (2) is confirmed via the great number of crystallized solvents which decrease the flexibility in the complex due to the different types of hydrogen bonds.⁴⁹ On the other hand, in comparison with complexes (3) and (4), it was declared that the stability order is: Co<Ni for complexes (3) and (4). The higher thermal stability of nickel is attributed to its smaller ionic radii and higher electronegativity than Co(II). Based on the above results the suggested chemical structure for all metal chelates is represented in (Fig. 2).

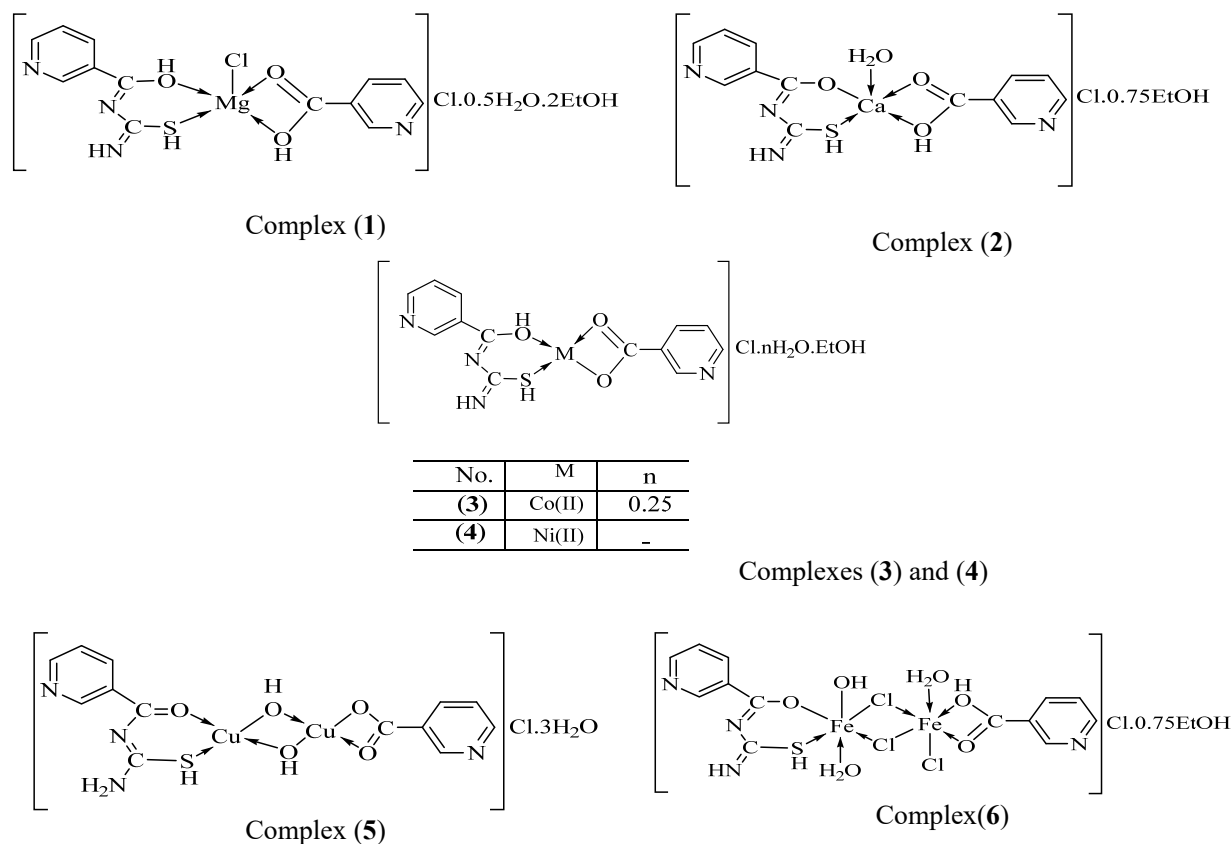


Fig. 2. Suggested chemical structures of metal chelates

Table 1. Thermal Analysis (TG/ DTG) Data for Nicotinic Acid, and Thiourea Metal Complexes

No.	Compound	TG range	DTG Peak	Mass Loss %		Assignments	T _s (°C)
		(°C)	(°C)	Calcd.	Found		
(1)	[Mg(C ₁₃ H ₁₂ N ₄ O ₃ S) Cl]Cl.0.5H ₂ O.2EtOH	20-163	88w	18.58	18.20	Loss of 1.25 mol of EtOH and 0.5 mol of Cl ₂ gas ^d	163
		163-320	228s	49.58	49.28		
		320-700	424 w.br	23.79	24.48	Loss of 0.5 mol of lattice H ₂ O and complete ligand pyrolysis ((CH ₆ N ₂ O ₂ S) ^d	
		At 700		8.05	8.05	MgO ^f	
(2)	[Ca(C ₁₃ H ₁₁ N ₄ O ₃ S)(H ₂ O)]Cl.0.75EtOH	30-123	54m	13.57	13.53	Loss of 0.5 mol of EtOH and 0.5 mol of Cl ₂ gas ^d	123
		123-327	209s	54.87	54.68	Loss of 0.25 mol of EtOH, one mol of coordinated H ₂ O, and partial ligand pyrolysis (C ₁₂ H ₇ N ₄) ^d	
		327-700	473w.br	17.17	17.05	Complete ligand pyrolysis (C _{0.5} H ₄ O ₂ S) ^d	
		At 700		14.39	14.74	(CaO+0.5C) ^f	
(3)	[Co(C ₁₃ H ₁₁ N ₄ O ₃ S) Cl.0.25H ₂ O. EtOH	20-248	–	2.57	2.64	Loss of 0.25 mol of EtOH ^b	248
		248-356	288s	36.95	36.80	Loss of 0.75 mol of EtOH, 0.25mol of H ₂ O, 0.5 mol of Cl ₂ gas, and partial ligand pyrolysis (C ₃ H ₃ N ₂) ^d	
		356-456	407m	20.77	21.40	Partial ligand pyrolysis (C ₆ H ₇ N) ^d	
		456-700	575m.br	15.84	14.56	Complete ligand pyrolysis (HNO _{1.5} S) ^d	
(4)	[Ni(C ₁₃ H ₁₁ N ₄ O ₃ S)Cl.EtOH	21-294	–	2.60	2.71	Loss of 0.25 mol of EtOH ^b	294
		294-700	374s.br	75.14	75.34	Loss of 0.75 mol of EtOH, 0.5 mol of Cl ₂ , and complete ligand pyrolysis (C ₁₁ H ₁₁ N ₄ O ₂ S) ^d	
		At 700		22.26	21.95	(NiO+2C) ^f	
(5)	[Cu ₂ (C ₁₃ H ₁₁ N ₄ O ₃ S) (OH) ₂]Cl.3H ₂ O	25-146	63m	16.16	16.17	Loss of 3 mol of crystallized H ₂ O, and 0.5 mol of Cl ₂ gas ^{a+b}	146
		146-380	300s	49.70	49.62	Partial ligand pyrolysis (C ₁₂ H ₁₁ N ₄ O ₂ S) ^d	
		380-700	401w	5.42	5.57	Complete ligand decomposition (CH ₂ O) ^d	
		At 700		28.72	28.64	(2CuO) ^f	
(6)	[Fe ₂ (C ₁₃ H ₁₁ N ₄ O ₃ S)Cl ₃ (OH)(H ₂ O) ₂]Cl.0.75EtOH	26-170	48w	5.36	5.30	Loss of 0.75 mol of EtOH ^b	170
		170-303	242s	32.92	32.88	Loss of 1.25 mol of coordinated H ₂ O, 0.5 mol of Cl ₂ gas, and partial ligand pyrolysis (C ₁₀ H ₆ N ₂) ^d	
		303-415	348m	18.63	18.18	Loss of 0.75 mol of coordinated H ₂ O, 0.5 mol of Cl ₂ gas, one mol of coordinated OH, and Partial ligand pyrolysis (C ₂ H ₂ N ₂) ^d	
		415-700	471s	18.32	18.94	Complete ligand pyrolysis (CH ₂ S) and loss of coordinated chloride ions (2Cl ⁻) ^d	
		At 700		24.77	24.70	(Fe ₂ O ₃) ^f	

Abbreviations: b: broad; m: medium; s: strong; w: weak; m.br: medium broad; s.br: strong broad; w.br: weak broad. a: dehydration; desolvation; d: decomposition and f: final residue

Table 2. Thermodynamic Data of the Thermal Decomposition of Metal Complexes

No.	Compound	DTG	Temperature	n	E*/ KJmol ⁻¹	ΔH*/ KJmol ⁻¹
		Peak (°C)	Range (°C)			
1	[Mg(C ₁₃ H ₁₂ N ₄ O ₃ S)Cl]Cl.0.5H ₂ O.2EtOH	88w	20 -163	1.26	22.29	19.39
		228s	163 -320	1.41	87.01	83.97
		424w.br	320 -700	1.17	122.18	121.53
2	[Ca(C ₁₃ H ₁₁ N ₄ O ₃ S)(H ₂ O)]Cl.0.75EtOH	54m	30-123	1.89	30.00	27.15
		209s	123-327	1.28	72.32	69.06
		473w.br	327-700	0.925	52.33	49.06
3	[Co(C ₁₃ H ₁₁ N ₄ O ₃ S)]Cl.0.25H ₂ O.EtOH	288s	248-356	0.824	25.48	22.87
		407m	356-456	1.82	47.37	44.68
		575m.br	456-700	1.12	23.29	20.03
4	[Ni(C ₁₃ H ₁₁ N ₄ O ₃ S)]Cl.EtOH	374s.br	294-700	1.18	21.44	18.51
5	[Cu ₂ (C ₁₃ H ₁₁ N ₄ O ₃ S)(OH) ₂]Cl.3H ₂ O	63m	25-146	1.74	30.79	27.94
		300s	146-380	1.13	61.64	58.7
		401w	380-700	1.41	58.48	55.44
6	[Fe ₂ (C ₁₃ H ₁₁ N ₄ O ₃ S)Cl ₃ (OH)(H ₂ O) ₂]Cl.0.75.EtOH	48w	26-106	1.9	18.78	16.03
		242s	106-303	0.85	54.19	51.4
		348m	303-415	1.45	125.19	122.36
		471ss	415-700	1.45	96.82	96.35

3.8. Agriculture Application

Nicotinic acid and thiourea complexes were evaluated for plant growth promoters on the (Wheat) plants. Results demonstrated that the maximum germination rate and green weight were recorded in a mixture of complexes,²⁸⁻³⁰ (Table 3, and Fig. 3).

Table 3. Illustrated the Effect of Different Treatment Concentrations on Germination Rate, Average Green, and Dry Weight, Nitrogen and Metal Concentrations

Treatment	Concentration (ppm)	Germination Rate (%)	Average green weight	Average dry weight	Nitrogen conc. (%)	Metal conc. (%)
Control	-	75.6	1.83	0.69	0.48	-
Mg (1)	50	93.6	3.41	1.26	8.18	0.44
	150	96.3	3.71	1.38	8.51	0.58
	250	92.6	3.40	1.19	8.18	0.40
Ca (2)	50	94	3.41	1.27	8.35	0.52
	150	94.6	3.64	1.34	8.427	1.07
	250	90.6	3.31	1.16	8.07	0.23
Fe (6)	50	96	3.71	1.36	8.46	1.9
	150	96.6	3.72	1.41	8.52	2.16
	250	90.3	3.23	1.12	8.04	0.88
Mix	50	94.1	3.42	1.29	8.42	Fe=1.26 Ca=0.90 Mg=0.55
	150	98.6	3.81	1.48	8.57	Fe=1.96 Ca=2.23 Mg=0.17
	250	90.1	3.12	1.12	7.98	Fe=2.29 Ca=2.63 Mg=0.16

3.9. Biological Activity

3.9.1. Antibacterial Activity

Different complexes (1, 2, and 3) were distributed to measure their antibacterial activity against *Erwinia carotovora* sbp. *carotovora*. The inhibition zones were measured with a millimeter ruler at the termination of the incubation period. Complex (6) demonstrates a good antibacterial activity than complexes (1) and (2) with an inhibition zone of 21.1 nm, (Table 4, and Fig. 4).

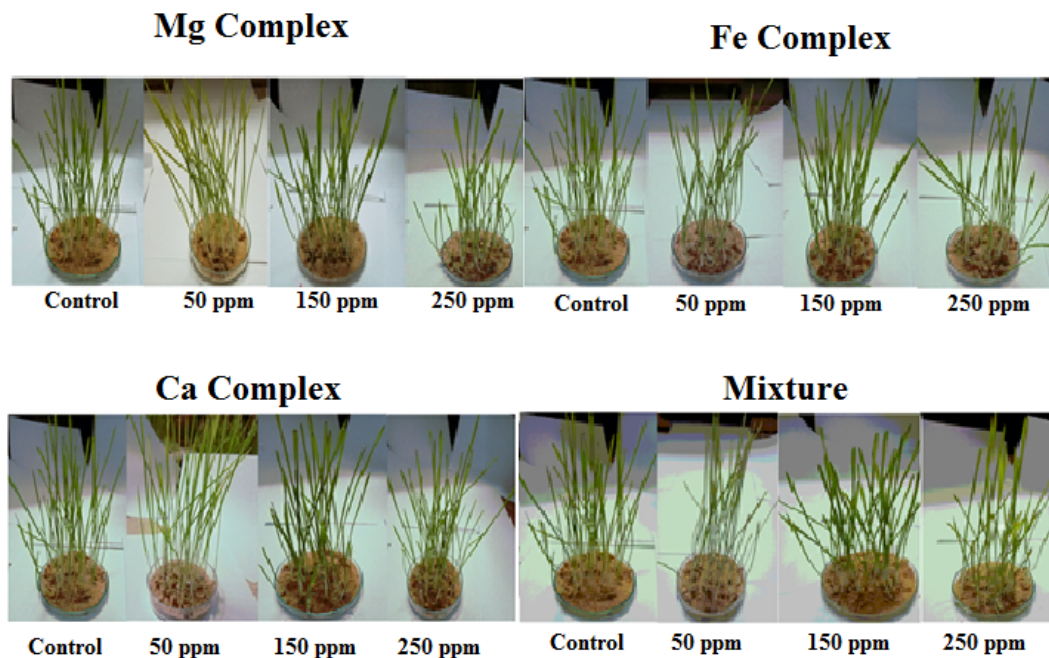


Fig. 3. Effect of Mg(II),Ca(II), Fe(III), and mixture of complexes on wheat plant

Table 4. Effect of different metal complexes concentrations on inhibition of *Erwinia carotovora* sp. *carotovora* on nutrient agar

Treatment	Concentration (ppm)	Radius inhibition zone (mm)	Inhibition %
Untreated control (sterile distilled water)	–	0.0	0.0
Mg (1)	200	0.0	0.0
	400	0.0	0.0
	600	15.0	16.6
	800	18.5	20.5
Ca (2)	200	0.0	0.0
	400	14.0	15.5
	600	15.0	16.6
	800	17.0	18.8
Fe (6)	200	0.0	0.0
	400	0.0	0.0
	600	17.0	18.8
	800	19.0	21.1
Mixture	200	0.0	0.0
	400	0.0	0.0
	600	0.0	0.0
	800	17.0	18.8
Treated control (<i>streptomycin</i>)	200	0.0	0.0
	400	14.0	15.5
	600	17.5	19.4
	800	24.0	26.7

3.9.2. Antifungal Activity

The growth inhibition was calculated after 10 days and the data are listed in (Table 5). The results showed that complex (6) displays perfect antifungal activity against *Fusarium oxysporum* f. sp. *betae* with inhibition zone 48.33% (Table 5, and Fig. 5) according to this equation:

$$\text{Growth inhibition (\%)} = [(R_1 - R_2) / (R_1)] \times 100$$

whereas R_1 = inward linear growth in the control plate and R_2 = inward linear growth in the treatment plate.

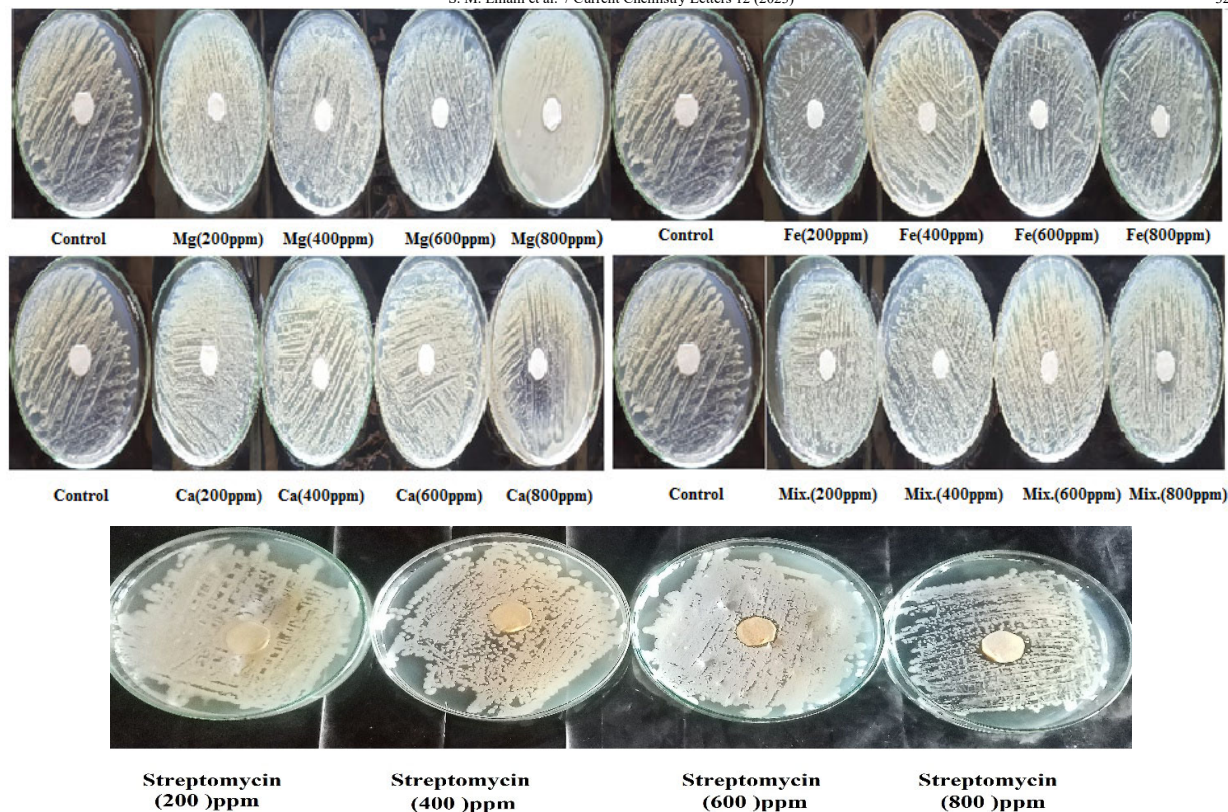


Fig. 4. Effect of different metal complexes concentrations on inhibition of *Erwinia carotovora* sp. *carotovora* on nutrient agar

Table 5. Effect of different metal complexes concentrations on inhibition of *Fusarium oxysporum* f.sp. *betae* on PDA

Treatment	Concentration (ppm)	Radial growth (mm)	Inhibition %
Untreated control (sterile distilled water)	–	90.0	0.0
Mg (1)	200	86.0	4.44
	400	78.0	13.33
	600	67.0	25.56
	800	58.0	35.56
Ca (2)	200	90.0	0.0
	400	90.0	0.0
	600	74.5	17.22
	800	70.0	22.22
Fe (6)	200	90.0	0.0
	400	76.0	15.56
	600	65.0	27.78
	800	46.5	48.33
Mixture	200	90.0	0.0
	400	90.0	0.0
	600	90.0	0.0
	800	90.0	0.0
Treated control (<i>Maxim</i>)	200	55.5	38.33
	400	45.0	50.00
	600	34.0	62.22
	800	30.0	66.67

The higher antimicrobial activity was due to the high electronegative and ionic radius of the Fe(III) ion. Transition metals with large ionic radii, and high electronegative decrease the effective positive charges on the metal complex molecules which facilitates their interaction with the highly sensitive cellular membranes towards the charged particles and enhanced antibiological activity.⁷⁰

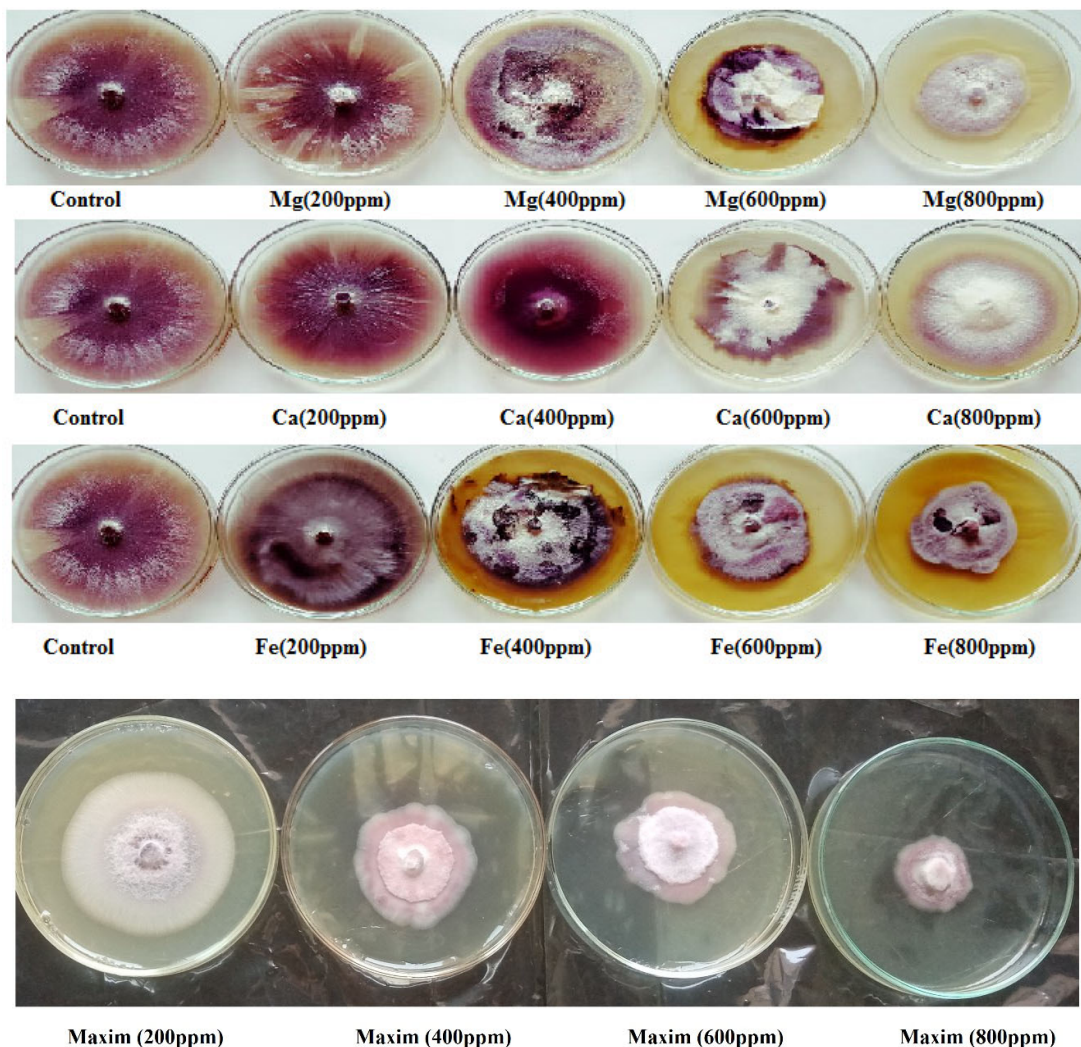


Fig. 5. Effect of various metal complexes concentrations on inhibition of *Fusarium oxysporum f.sp. betae* on potato dextrose agar

4. Conclusion

The appropriate metal chelates with various stoichiometries were produced when nicotinic acid and thiourea reacted with various metal chloride salts. Physicochemical investigations helped to establish the structure of metal complexes. In the chelates (1), (2), (3), and (4), the organic compound is tetradentate and linked to the metal through the carbonyl group, the protonated or deprotonated OH of the nicotinoyl moiety, and the SH group, while it coordinated in bidentate ligand in complexes (5) and (6), respectively. The electronic spectra displayed tetrahedral geometrical structure for complexes (3), and (4); square-planar, and high-spin octahedral structure for complexes (5), and (6), respectively.

The size of the transition metal and the number of solvent molecules influence the thermal stability of different metal chelates. TGA showed that the development of metal oxide or metal oxide contaminated with carbon was the ultimate result of the thermal breakdown. The antibacterial and agricultural applications make clear that complex (6) has the highest germination rate and green weight and is more effective against *Fusarium oxysporum f.sp. betae* and *Erwinia carotovora* sp. *carotovora*.

References

1. Fazal A. E., Yu. Y. H., Rajhi A. Q., Ayed S. A., Mohammad Y. A., Alshehri M. A., Kamel A. S., Elbehairi S. E. I., Fawy K. F., and Abd-Rabboh H. S. M. (2016) Bioactivities of novel metal complexes involving B vitamins and glycine, *Open Chem.*, 14, 287–298.
2. loyd-Jones D. M. (2014) Niacin and HDL cholesterol - time to face facts, *N. Engl. J. Med.* 371, 271–273.

3. Hussein M. M., Faham S. Y., and Alva A. K. (2014) Role of foliar application of nicotinic acid and tryptophan on onion plants response to salinity stress, *J. Agric. Sci.*, 6, 41–51.
4. Kumar V. (2009) Synthesis and anticancer activity of pyrido[2,3-c]pyridazine derivatives, *J. Sci. Islam. Repub. Iran*, 20, 325–329.
5. Bhojak N. (2017) A review on coordination behavior and bioactivity of metal complexes of nicotinic acid and its derivatives, *World J. Pharm. Pharm. Sci.*, 6, 490–514.
6. Paruch K., Biernasiuk A., Khylyuk D., Paduch R., Wujec M., and Popiolek Ł. (2022) Synthesis, biological activity and molecular docking studies of novel nicotinic acid derivatives, *Int. J. Mol. Sci.*, 23, 2823-2845.
7. Amuthalakshmi S., Ramalakshmi N., Arunkumar S., and Prabakaran A. (2022) Design, Synthesis, docking, characterization and biological screening of novel azetidinone derivatives of nicotinic acid, *Curr. Bioact. Compd.*, 18, 26-36.
8. Mohanram I., Meshram J., Kandpal B., Shaikh A., and Deshpande S., (2013) Synthesis of novel anti-inflammatory and antimicrobial agents via Ugi-4CR and its evaluation, *J. Appl. Pharm. Sci.*, 3, 057-061.
9. Narang R., Narasimhan B., Sharma S., Sriram D., Yogeewari P., Clercq E., Pannecouque C., and Balzarini J. (2012) Synthesis, antimycobacterial, antiviral, antimicrobial activities and QSAR studies of nicotinic acid benzylidene hydrazide derivatives, *Med. Chem. Res.*, 21, 1557–1576.
10. Ma L., Zwahlen R. A., Zheng L.W. and Sham M. H. (2011) Influence of nicotine on the biological activity of rabbit osteoblasts, *Clin. Oral Impl. Res.*, 22, 338-342.
11. Zalaa M., Voraa J. J., and Patel H. B. (2020) Synthesis, characterization, and comparative study of some heterocyclic compounds containing isoniazid and nicotinic acid hydrazide moieties, *Russ. J. Org. Chem.*, 56, 1795–1800.
12. Jain N., Utreja D., and Dhillon N. K. (2019) A convenient one-pot synthesis and nematocidal activity of nicotinic acid amides, *Russ. J. Org. Chem.*, 55, 845–851.
13. Damian D. L. (2017) Nicotinamide for skin cancer chemoprevention, *Austr. J. Dermatol.*, 58, 174–180.
14. Bourgin M., Kepp O., and Kroemer G. (2022) Immunostimulatory effects of vitamin B₅ improve anticancer immunotherapy, *OncImmunology*, 11(1), 203-209.
15. Smith G., and Wermuth U. D. (2010) Three-dimensional hydrogen-bonded structures in the 1:1 proton-transfer compounds of l-tartaric acid with the associative-group monosubstituted pyridines 3-amino-pyridine, 3-carboxy-pyridine (nicotinic acid) and 2-carboxy-pyridine (picolinic acid), *Acta Crystallogr. C* 66, 5-10.
16. Hasanin M., and Labeeb A. M. (2021). Dielectric properties of nicotinic acid/methylcellulose composite via “green” method for anti-static charge applications. *Mater. Sci. Eng. C: B*, 263, 114797-114806.
17. Alesary H. F., Ismail H. K., Odda A. H., Watkins M. J., Majhool A. A., Ballantyne. D., and Ryder K. S. (2021) Influence of different concentrations of nicotinic acid on the electrochemical fabrication of copper film from an ionic liquid based on the complexation of choline chloride-ethylene glycol. *J. Electroanal. Chem.*, 897, 115581-115591.
18. Hosseinzadeh S. F., and Mokhtary, M., (2018). Application of nicotinic acid functionalized chlorosulfonic acid as a green catalyst for the synthesis of bis (2-methyl-1-indole) derivatives. *J. Appl. Chem. Res.* 12(3), 31-41.
19. Li S., Li H., Cao X., and Chen C. (2013) Synthesis and bio-evaluation of novel salicylic acid-oriented thiourea derivatives with potential applications in agriculture, *Lett. Drug Des. Discov.*, 11, 98–103.
20. Wahid A., Basra S. M. A., and Farooq M., (2017) Thiourea: A molecule with immense biological significance for plants, *Int. J. Agric. Biol.*, 19, 911–920.
21. Min L.-J., Zhai Z.-W., Shi Y.-X., Han L., Tan C.-X., Weng J.-Q., Li B. J., Zhang Y.-G., and Liu X.-H., (2019) Synthesis and biological activity of acyl thiourea containing difluoromethyl pyrazole motif, *Phosphorus Sulfur Silicon Relat. Elem.*, 195, 22-28.
22. Venkataramana L.R., Reddy A. V. K., Swetha V., Zyryanov G. V., and Raju C. N. (2022) Synthesis and bio-activity studies of urea/thiourea derivatives of 4,4'-diamino diphenyl methane, *Conf. Proc.*, 2390, 85-96.
23. Kholodniak O., and Kovalenko S., (2022) Substituted acyl thioureas and acyl thiosemicarbazides: Synthesis and biological activity (minireview), *Pharm. Sci.*, 2, 56-71.
24. Tok F., Cakir C., Cam D., Kirpat M.M., and Sicak Y. (2022) Synthesis, characterization and biological evaluation of novel thiourea derivatives, *Clin. Exp. Health Sci.*, 12, 533-540.
25. Shoukat M.R., Leghari S.J., Ahmad N., Virk A.L., and Haider F. U. (2022) Effects of foliar applied thiourea on maize physiology, growth and yield (*Zea mays* L.) under shaded conditions, *J. Plant Nutr.*, 45, 1312-1321.
26. Groenewald T., (1977). Potential applications of thiourea in the processing of gold *J. South Afr. Inst. Min. Metall.*, 77(11), 217-223.
27. Loto R. T., Loto C. A. and Popoola A. P. I. (2012). Corrosion inhibition of thiourea and thiadiazole derivatives: a review, *J. Mater. Environ. Sci.*, 3(5), 885-894.
28. Shahid M., Shukla A. K., Bhattacharyya P., Tripathi R., Mohanty S., Kumar A., Lal B., Gautam P., Raja R., Panda B. B., Das B., and Nayak A. K. (2016) Micronutrients (Fe, Mn, Zn, and Cu) balance under long-term application of fertilizer and manure in a tropical rice-rice system. *J. Soils Sediments*, 16(3), 737–747.
29. Snowball K., and Robson A. D. (1991) Nutrient Deficiencies and Toxicities in Wheat: A Guide for Field Identification, *Nutr. Defic. Toxicities Wheat*, 1-76.
30. El-Megharbel S. M., Refat M. S., Al-Salmi F. A., and Hamza R. Z., (2021). In Situ neutral system synthesis, spectroscopic, and biological interpretations of magnesium(II), calcium(II), chromium(III), zinc(II), copper(II), and selenium(IV) sitagliptin complexes. *Int. J. Environ. Res. Public Health*, 18, 1-19.

31. Billet K., Malinowska M. A., Munsch T., Unlubayir M., Adler S., Delanoue G., and Lanoue A. (2020) Semi-targeted metabolomics to validate biomarkers of grape downy mildew infection under field conditions, *Plants*, 9(9), 1008-1025.
32. Billet K., Unlubayir M., Munsch T., Malinowska M. A., Bernonville T. D., Oudin A., Courdavault V., Besseau S., Giglioli-Guivarc'h N., and Lanoue A. (2021), *ACS Sustain. Chem. Eng.*, 9(8), 3509-3517.
33. Bassett J., Denney R. C., Jeffery G. H., and Mendham J. (1978) *Vogel's Textbook of Quantitative Inorganic Analysis Including Elementary Instrumental Analysis*, 4th ed. Longman Group, London.
34. Lewis J., and Wilkins R. G. (1960) *Modern Coordination Chemistry, Principles and Methods*, Interscience New York, 403.
35. Elsayed Y., and Shabana Y. (2018) The effect of some essential oils on *Aspergillus niger* and *Alternaria alternata* infestation in archaeological oil paintings, *Mediterr. Archaeol. Archaeon*, 18, 71–87.
36. Shawki K., Elsayed A., Abido W., and Shabana Y. (2020) Using green chemicals and biological control agents for controlling the Seed-Borne Pathogen *Fusarium moniliforme* in Sugar Beet, *J. Plant Prot. Pathol.*, 11, 63–72.
37. Yuen S. H., and Pollard A. G. (1953) Determination of nitrogen in the soil and plant materials: Use of boric acid in the micro-Kjeldahl method, *J. Sci. Food Agric.*, 4, 490–496.
38. Geary W. J. (1971) The use of conductivity measurements in organic solvents for the coordination compounds, *Coord. Chem. Rev.*, 7, 81-122.
39. Abouzayed F. I., Emam S. M., and Abuel-Enein S. A. (2020) Synthesis, characterization and biological activity of nano-sized Co(II), Ni(II), Cu(II), Pd(II) and Ru(III) complexes of tetradentate hydrazine ligand, *J. Mol. Struct.*, 1216, 128314-128326.
40. Sanina N. A., Aldoshin S.M., Shmatko N. Y., Korchagin D. V., Shilov G. V., Ovanesyan N. S., and Kulikov A. V. (2014) Mesomeric tautomerism of ligand is a novel pathway for synthesis of cationic dinitrosyl iron complexes: X-ray structure and properties of nitrosyl complex with thiourea, *Inorg. Chem. Commun.*, 49, 44–47.
41. Stewart J. E. (1957) Infrared absorption spectra of urea, thiourea and some thiourea-alkali halide complexes, *J. Chem. Phys.*, 26, 248-254.
42. Struktur K., Siri S., and Pivaloiltiourea T. (2011) Spectroscopic and structural study of a series of pivaloylthiourea derivatives, *Malaysian J. Anal. Sci.*, 15, 37–45.
43. Ragamathunnisa R. N., Rani J. V., Padmavathy R., and Radha N. (2013) Spectroscopic study on thiourea and thiosemicarbazide in nonaqueous media, *IOSR J. Appl. Phys.*, 4, 5–08.
44. Emam S.M. (2017) Spectral characterization, thermal and biological activity studies of Schiff base complexes derived from 4,4'-methylenedianiline, ethanol amine and benzyl, *J. Mol. Struct.*, 1134, 444-457.
45. Rao C. N. R., Venkataraghavan R., and Kasturi T. R. (1964) Contribution to the infrared spectra of organosulfur compounds, *Can. J. Chem.*, 42, 36–42.
46. Gadag R. V., and Gajendragad M. R. (1978) Complexes of Cu(I), Ag(I), Ti(I), Zn(I), and Cd(II) with 3-methyl,3-ethyl derivatives of 4-amino-5-mercapto-1,2,4-triazole, *Indian J. Chem.*, 16A, 703–705.
47. Cinarli A., Gürbüz D., Tavman A., and Birteksöz A. (2011) Synthesis, spectral characterizations and antimicrobial activity of some Schiff bases of 4-chloro-2-aminophenol, *Bull. Chem. Soc.*, 25, 407–417.
48. Hassan A. M., Elbially Z. I., and Wahdan K. M. (2020) Study of antioxidant and anticorrosion activity of some microwave synthesized thiourea derivative ligands and complexes, *Sch. Int. J. Chem. Mater. Sci.*, 3, 83-98.
49. Emam S. M., Abou El-Enein S. A., and Emara E. M. (2017) Spectroscopic studies and thermal decomposition for bis((E)-2-(4-ethylphenylimino)-1,2-diphenylethanone) Schiff base and its Co(II), Ni(II), Cu(II), Zn(II) and Cd(II) complexes prepared by direct and template reactions, *J. Therm. Anal. Calorim.*, 127, 1611–1630.
50. Refat M.S., Altalhi T., and Hassan R. F. (2021) Synthesis, spectroscopic, structural and morphological characterizations of magnesium(II), calcium(II), strontium(II) and barium(II) folate complexes, *J. Mol. Struct.*, 1227, 519-524.
51. El Metwally N. M., Arafa R., and El-Ayaan U. (2014) Molecular modeling, spectral, and biological studies of 4-formylpyridine-4-N-(2-pyridyl)thiosemicarbazone (HFPTS) and its Mn(II), Fe(III), Co(II), Ni(II), Cu(II), Cd(II), Hg(II), and UO₂(II) complexes, *J. Therm. Anal. Calorim.*, 115, 2357–2367.
52. Ikram M., Rehman S., Islam N. U., and Jan N. (2011) Synthesis and characterization of Ni(II), Cu(II) and Zn(II) tetrahedral transition metal complexes of modified hydrazine, *J. Mex. Chem. Soc.*, 55, 164–167.
53. Alzamil N. O. (2020) Synthesis, DFT calculation, DNA-binding, antimicrobial, cytotoxic and molecular docking studies on new complexes VO(II), Fe(III), Co(II), Ni(II) and Cu(II) of pyridine Schiff base ligand, *Mater. Res. Express*, 7, 401-419.
54. Emam S. M., El-Tabl A. S., Ahmed H. M., and Emad E. A. (2014) Synthesis, structural characterization, electrochemical and biological studies on divalent metal chelates of a new ligand derived from pharmaceutical preservative, dehydroacetic acid, with 1,4-diaminobenzene, *Arab. J. Chem.*, 16(S2), S3816–S3825.
55. Emam S. M., El Sayed I. E. T., and Nassar N. (2015) Transition metal complexes of neocryptolepine analogs. Part I: Synthesis, spectroscopic characterization, and in vitro anticancer activity of copper (II) complexes, *Spectrochim. Acta A* 138, 942–953.
56. El-Samanody E. S. A., Emam S. M., and Emara E. M. (2017) Synthesis, characterization, molecular modeling and biological activity of metal complexes derived from (E)-N'-(furan-2-ylmethylene)morpholine-4-carbothiohydrazide, *J. Mol. Struct.*, 1146, 868–880.

57. Emam S. M., Abouel-Enein S. A., and Abdel-Satar E. M. (2019) Structural characterization, thermal investigation and biological activity of metal complexes containing Schiff Base ligand (Z)-3-(1-((4,6-dimethyl-1H-pyrazolo[3,4-b]pyridine-3-yl)imino)ethyl)-4-hydroxy-6-methyl-2H-pyran-2-one, *Appl. Organomet. Chem.*, 33, e4847– e4871.
58. Emam S. M., Abouel-Enein S. A., El-Saied F. A., and Alshater S. Y. (2012) Synthesis and characterization of some bi, tri and tetravalent transition metal complexes of N'-(furan-2-yl-methylene)-2-(p-tolylamino acetohydrazide HL1 and N'-(thiophen-2-yl-methylene)-2-(p-tolylamino)acetohydrazide HL², *Spectrochim. Acta A* 92, 96–104.
59. Ramadan A. M., Alshehri A. A., and Bondock S. (2019) Synthesis, physicochemical studies and biological evaluation of new metal complexes with some pyrazolone derivatives, *J. Saudi. Chem. Soc.*, 23, 1192–1205.
60. Gonc E. M., Bernardes C. E. S., Diogo P., and Minas M. E. (2010) Energetics and structure of nicotinic acid (Niacin), *J. Phys. Chem. B*, 114, 5475–5485.
61. Al-Qadsy I., Al-Odayni A.B., Saeed W. S., Alrabie A., Al-Adhrai A., Al-Faqeeh L. A. S., Lama P., Alghamdi A. A., and Farooqui M. (2021) Synthesis, characterization, single-crystal x-ray structure and biological activities of [(Z)-N'-(4-methoxybenzylidene)benzohydrazide–nickel(II)] complex, *Crystals* 11, 110-115.
62. Emam S. M., Tolan D. A., and El-Nahas A. M. (2020) Synthesis, structural, spectroscopic, and thermal studies of some transition-metal complexes of a ligand containing the amino mercapto triazole moiety, *Appl. Organomet. Chem.*, 34, 1–26.
63. Momo P. B., Leveille A. N., E. Farrar H. E., Grayson M. N., Mattson A. E., and Burtoloso A. C. B. (2020) Enantioselective S–H insertion reactions of α -carbonyl sulfoxonium ylides, *Angew. Chem. Int.*, 132, 15684-15689.
64. Abdel M. S., Ghorab M. M., Alsaied M. S., and Alqasoumi S. I., Design, (2016) Synthesis and anticancer evaluation of some novel thiourea, carbamimidothioic acid, oxazole, oxazolidine and 2-amino-1-phenylpropy-2-chloroacetate derived from L norephedrine, *Russ. J. Bioorg. Chem.*, 42, 434–440.
65. Piloyan G. O., Ryabchikov I. D., and Novikova O. S. (1966) Determination of activation energies of chemical reactions by differential thermal analysis, *Nature* 212, 1229-1229.
66. Melling R., Wilburn F. W., and Mcintosh R. M. (1969) Study of thermal effects observed by differential thermal analysis: Theory and its application to influence of sample parameters on a typical DTA curve, *Anal. Chem.*, 41, 1275–1286.
67. Alaghaz A. M. A., Zayed M. E., Alharbi S.A., and Ammar R.A.A. (2015) Synthesis, spectroscopic identification, thermal, potentiometric and antibacterial activity studies of 4-amino-5-mercapto-S-triazole Schiff's base complexes, *J. Mol. Struct.*, 1087, 60-67.
68. Gaber A., Refat M. S., Belal A.A.M., El-Deen M., Hassan N., Zakaria R., Alhomrani M., Alamri A., Alsanie W. F., and Saied E. M. (2021) New mononuclear and binuclear Cu(II), Co(II), Ni(II), and Zn(II) thiosemicarbazone complexes with potential biological activity: antimicrobial and molecular docking study, *Molecules* 26, 2288-2305.
69. El-Nahass M. N., Bakr E. A., El-Gamil M. M., and Ibrahim S. A. (2022) Synthesis, characterization, and multifunctional applications of novel metal complexes based on thiazolylazo dye, *Appl. Organomet. Chem.*, 36, 6625-6651.
70. Negm N.A., Zaki M.F., and Salem M.A.I. (2010) Cationic Schiff base amphiphiles and their metal complexes: Surface and biocidal activities against bacteria and fungi, *Colloids Surf. B: Biointerfaces*, 77, 96–103.



© 2023 by the authors; licensee Growing Science, Canada. This is an open access article distributed under the terms and conditions of the Creative Commons Attribution (CC-BY) license (<http://creativecommons.org/licenses/by/4.0/>).